Electronic structure, chemical bonding, and magnetic properties in the intermetallic series $Sc_2Fe(Ru_{1-x}Rh_x)_5B_2$ from first principles

German D. Samolyuk,[1] Boniface P. T. Fokwa,[2] Richard Dronskowski,[2] and Gordon J. Miller[1]
[1]*Department of Chemistry, Iowa State University, Ames, Iowa 50011, USA*
[2]*Institute of Inorganic Chemistry, RWTH Aachen University, Landoltweg 1, 52056 Aachen, Germany*
(Received 10 January 2007; revised manuscript received 6 June 2007; published 10 September 2007)

First-principles, density-functional studies of the electronic structure, chemical bonding, ground-state magnetic ordering, and exchange-interaction parameters have been performed for the entire $Sc_2Fe(Ru_{1-x}Rh_x)_5B_2$ series of magnetic compounds. The results indicate that their magnetic properties depend in an extremely sensitive way on the degree of band filling and bandwidth. Continuous substitution of Ru by Rh changes the ground state from an antiferromagnet to a ferromagnet, as well as increases the effective spin moment caused by filling the bands with five additional electrons per formula unit together with a narrowing of the 4*d* band. The correlations between the character of the chemical bonding and the resulting exchange couplings are discussed. The enhancement of Fe-Fe exchange coupling caused by Rh/Ru atoms is estimated. Trends for the macroscopic ordering temperatures are correctly reproduced.

DOI: 10.1103/PhysRevB.76.094404 PACS number(s): 75.50.Cc, 71.15.Mb, 71.20.Lp, 75.30.Et

I. INTRODUCTION

During the last decade, a number of quaternary intermetallic borides with the general formula $M_2M'T_5B_2$ (M=Mg or Sc; M'=main-group metal or 3*d* element; T=Ru, Rh, Ir) crystallizing in the space group $P4/mbm$ have been synthesized and structurally characterized.[1–3] Among these compounds, those with magnetically active 3*d* elements Mn, Fe, Co have attracted increased interest because they exhibit ferromagnetic or antiferromagnetic behavior that can be fine-tuned by synthetic means. In addition, the magnetically active 3*d* metal atoms form well separated, one-dimensional chains. Thus, the question arises whether these compounds show low-dimensional, itinerant magnetism, which offers potential application for data storage and retrieval.

From a theoretical perspective, the use of quantum-chemical bond detecting tools such as the crystal orbital hamilton population (COHP)[4] analysis made it possible to understand, from a chemical perspective, the nature of the magnetic behavior in some of these compounds as it was shown to be solely a function of the electron count.[5] Among $M_2M'T_5B_2$ examples, ferromagnets turned out to have 65 valence electrons (e.g., $Sc_2FeRh_5B_2$) with the Fermi level falling within metal-metal antibonding states, whereas antiferromagnets, e.g., $Mg_2MnRh_5B_2$, have 62 valence electrons, where the Fermi level falls within metal-metal nonbonding states. These findings also allowed further experimental search for new ferromagnets and antiferromagnets, and successfully led to the discovery of both $Sc_2MnRu_2Rh_3B_2$ and $Sc_2FeRu_3Rh_2B_2$. These derivatives are conveniently formulated as $M_2M'(T_{1-x}T'_x)_5B_2$, so that there is chemical choice among the 4*d* (T,T') metal sites to adjust the number of valence electrons. These two isotypic compounds both contain 62 valence electrons and, as predicted, both are itinerant antiferromagnets.[5,6]

The magnetic properties and exchange couplings of related magnetic systems, i.e., FeRh and FePt, have been studied[7–9] and provide differing opinions on how to treat the Rh or Pt magnetic moments in such systems. The results of noncollinear magnetic calculations[7,8] show that the magnetic moment at the Fe site is essentially localized and can be described according to a rigid-spin approximation, while the Rh or Pt magnetic moments are delocalized and determined, both in direction and magnitude, by the exchange field from the Fe moments. To describe these systems with both localized and delocalized magnetic degrees of freedom, an effective spin Hamiltonian model was developed.[7,8] In this model, the localized Fe magnetic moments are described by a Heisenberg Hamiltonian and the itinerant moments within a Stoner model, in which the magnetic moments of Rh or Pt atoms are induced by the Fe exchange field. This description quantitatively reproduces the experimentally observed anomaly in the temperature dependence of the magnetic anisotropy energy. On the other hand, a standard Heisenberg model with rigid spins for both Fe and Rh moments in FeRh reproduced the phase transition temperatures of both antiferromagnetic-to-ferromagnetic and ferromagnetic-to-paramagnetic phase transitions in reasonable agreement with experiment.[9]

In the present publication, we investigate the local nature of the exchange interactions in $Sc_2Fe(Ru_{1-x}Rh_x)_5B_2$ to examine the relationship between effective exchange coupling and metal-metal COHP in these itinerant magnets. Our calculations of exchange couplings are based on the linear-response technique[10–13] in the long wavelength approximation.[14] Two models are used to describe the magnetic properties of $Sc_2Fe(Ru_{1-x}Rh_x)_5B_2$. In the first case ("model 1"), we treated the magnetic moments at both the Fe and Rh/Ru sites as independent rigid moments together with the usual assumption of weak enhancement of magnetic exchange parameters (J_{ij}).[14] We obtain J_{ij} values for a number of $Sc_2Fe(Ru_{1-x}Rh_x)_5B_2$ compounds from first principles, and then analyze how the mechanism of the magnetic coupling depends on electronic structure variations induced by atomic substitution. In particular, we will arrive at results that are similar to our previous treatments for Heusler alloys[15] and to published results for FePt and FeRh.[7–9] In $Sc_2Fe(Ru_{1-x}Rh_x)_5B_2$, the 4*d*-3*d* Rh/Ru-Fe interactions yield

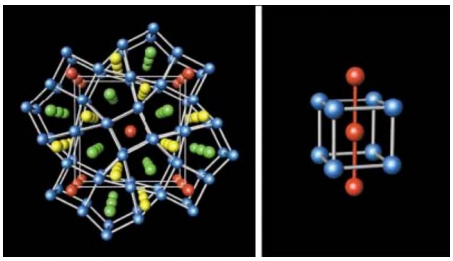

FIG. 1. (Color online) (Left) Perspective view of the crystal structure of the series $M_2M'T_5B_2$ along the c axis, and (right) a tetragonal prism of T atoms surrounding the M' atoms. M sites are green spheres, M' sites are red spheres, T sites are blue spheres, and B sites are yellow spheres.

larger, even leading contributions to the total effective coupling of the Fe atoms as compared to the 3*d*-3*d* Fe-Fe interactions. In the second model ("model 2"), we treated just the Fe magnetic moments as independent. However, to calculate the Fe-Fe exchange parameters, we used the total magnetic susceptibility χ_{ij}^{+-}, rather than the "bare" magnetic susceptibility $\chi_{ij}^{(0)+-}$,[14] which has been traditionally used for such calculations. In this case, the total susceptibility χ_{ij}^{+-} includes enhancement effects caused by Rh/Ru sites.

Finally, numerical calculations targeted at finite-temperature properties such as Curie (T_C) and Néel (T_N) ordering temperatures are performed on the basis of a direct, exchange-based approach. Because the mean-field approximation (MFA) usually overestimates critical temperatures in systems with few nearest neighbors, we also used the cluster variation method (CVM)[16,17] to calculate critical temperatures for some concentrations. CVM typically gives agreement within 5%–10% with results of more accurate spin dynamics procedures, even in such a systems such as dilute magnetic semiconductors,[17] where MFA overestimates T_C by a factor of 2.

In summary, this contribution attempts to provide an essentially chemical understanding of bonding and magnetic exchange parameters starting from ideas touching upon elementary body-centered cubic 3*d* metals such as α-Fe and continuing these ideas for the quaternary intermetallic borides as done in Refs. 15 and 18.

II. CRYSTAL STRUCTURE AND COMPUTATIONAL DETAILS

All quaternary intermetallic borides with the general formula $M_2M'T_5B_2$ (Refs. 1–3) crystallize with an ordered variant of the $Ti_3Co_5B_2$ aristotype.[10] As shown in Fig. 1, this structure contains trigonal, tetragonal, and pentagonal prisms of the T (Co) atoms stacked on top of each other along the [001] direction. The trigonal prisms enclose the B atoms, while the pentagonal prisms accommodate the M atoms and the tetragonal prisms (cubes) contain the M' atoms. The M' atoms are arranged in chains along the [001] direction (see Fig. 1, right) with intrachain M'-M' distances of about 3.0 Å and interchain distances of about 6.6 Å.[19]

The electronic structures of $Sc_2Fe(Ru_{1-x}Rh_x)_5B_2$ were calculated using the tight-binding, linear muffin-tin orbital method with the atomic-spheres approximation (LMTO-ASA).[20,21] The exchange-correlation term was calculated both within the local-spin-density approximation (LSDA), which was parametrized according to von Barth and Hedin,[22] and the generalized gradient approximation (GGA) with the Perdew-Burke-Ernzerhof functional[23] for the experimental values of the lattice parameters. A mesh of 54 k points in the irreducible wedge of the Brillouin zone (BZ) turned out to be sufficient for the calculations of the exchange parameters. To treat different concentrations of Ru and Rh quantitatively, we used ordered distributions of these elements within the experimental unit cells. The sizes of atomic sphere radii for our calculations are Ru1/Rh1, 2.70–2.72 Å; Ru2/Rh2, 2.60–2.62 Å; Sc, 3.31–3.20 Å; Fe, 3.12–3.04 Å; B, 2.17–2.15 Å.

The chemical bonding was investigated using the COHP analysis, which is an energy-resolved partitioning technique of the band-structure energy (sum of the Kohn-Sham eigenvalues) in terms of atomic and bonding contributions. After the electronic structure calculations have been brought to full self-consistency, an energy-partitioning method is utilized to separate the entire band-structure energy into specified interatomic interactions (the COHP) given that an atom-centered basis set (such as LMTOs) has been provided. In other words, the delocalized electronic structure calculated in reciprocal space is exactly transformed into real space; in addition, the result of this transformation is presented in an energy-resolved form, i.e., as a function of band filling. Experience shows that, within stable materials, nature maximizes the integrated COHP values for the strongest bonds by annihilating antibonding states such as to avoid Jahn-Teller or Peierls instabilities.

For the prediction of ferro—or antiferromagnetic spin ordering in magnetic intermetallics, the COHP is calculated using a non-spin-polarized state and analyzed for the highest filled states, i.e., at the Fermi level. Whenever atom-atom interactions turn out to be strongly antibonding at the Fermi level for those metals which show strong exchange splitting (i.e., the 3*d* metals), the material is likely to spin polarize and order ferromagnetically, as seen for α-Fe [body-centered cubic (bcc)]. If the atom-atom interactions are nonbonding at the Fermi level (such as in bcc-Cr), the material will exhibit antiferromagnetic ordering.

The general theoretical strategy to evaluate the local effective exchange parameters in the long wavelength approximation with an assumption of weak enhancement[14] has already been discussed in Ref. 24. These effective exchange parameters are used to calculate the thermal properties[11] of magnets, and are derived from the pairwise exchange interactions, J_{ij}, which explicitly enter the Heisenberg Hamiltonian,

$$H = -\sum_{i,j}{}' J_{ij}\mathbf{e}_i \cdot \mathbf{e}_j, \tag{1}$$

where i and j are indices of atoms, and $\mathbf{e}_i$ and $\mathbf{e}_j$ are the directions of the local magnetic moments at atoms i and j.

For model 1, the J_{ij} values are obtained using multiple scattering theory according to

$$J_{ij} = \frac{1}{2\pi}\int^{E_F} d\varepsilon \,\mathrm{Im} \sum_{L,L'} \{\delta P_{i,l}(\varepsilon)[T^{\uparrow}_{i,L;j,L'}(\varepsilon)T^{\downarrow}_{j,L';i,L}(\varepsilon) + T^{\downarrow}_{i,L;j,L'}(\varepsilon)T^{\uparrow}_{j,L';i,L}(\varepsilon)]\delta P_{j,l'}(\varepsilon)\}, \quad (2)$$

where $\delta P_{i,l}(\varepsilon)$ is the on-site perturbation on atom i for orbital momentum l and $T^{\sigma}_{ij}(\varepsilon)$ is the scattering-path operator connecting atoms i and j, dependent on the complex energy ε for the channel with spin σ ($\uparrow$ or $\downarrow$) and L stands for the orbital momentum and its projection (l,m). Details of this calculation are summarized in Appendix A. For the assumption that all potential parameters used to calculate $\delta P_{i,l}(\varepsilon)$ are equal for spin "up" and "down" except the band centers, the expression for J_{ij} can be reduced to $J_{ij}=-\Delta_i(\chi^{+-}_{ij}+\chi^{-+}_{ij})\Delta_j$ and $\chi^{+-}_{ij}=-\mathrm{Im}\int^{E_F}G^{\uparrow}_{ij}(\varepsilon)G^{\downarrow}_{ji}(\varepsilon)d\varepsilon/(2\pi)$ (see Ref. 25 and Appendix A for the details).

Alternatively (model 2), we calculate Fe-Fe J_{ij} values using the static transverse susceptibility χ^{+-}_{ij}.[14] The connection between "susceptibility" and the expressions for J_{ij} from multiple scattering theory is discussed in Sec. III A. The expression for χ^{+-}_{ij} is[26]

$$\chi^{+-}_{ij} = \chi^{(0)+-}_{ij} + \sum_k \chi^{(0)+-}_{ik} I_k \chi^{+-}_{kj} + \sum_\alpha \chi^{(0)+-}_{i\alpha} I_\alpha \chi^{+-}_{\alpha j},$$

$$\chi^{+-}_{\alpha i} = \chi^{(0)+-}_{\alpha i} + \sum_k \chi^{(0)+-}_{\alpha k} I_k \chi^{+-}_{ki} + \sum_\beta \chi^{(0)+-}_{\alpha\beta} I_\beta \chi^{+-}_{\beta i}, \quad (3)$$

where indices i, j correspond to Fe atoms, α, β to Rh/Ru atoms. I_α (I_β) are parameters that can be approximated by the Stoner exchange integral, i.e., ~650 meV for Rh, 600 meV for Ru,[27] and $\chi^{(0)+-}_{ij}$ is the bare susceptibility usually used for calculating J_{ij} values. The formal expression for χ^{+-}_{ij} can be obtained from the system of equations (3) in the form

$$\chi^{+-}_{ij} = \tilde{\chi}^{(0)+-}_{ij} + \sum_k \tilde{\chi}^{(0)+-}_{ik}[\delta_{kj} - I_k\tilde{\chi}^{(0)+-}_{kj}]^{-1},$$

$$\tilde{\chi}^{(0)+-}_{ij} = \chi^{(0)+-}_{ij} + \sum_\alpha \chi^{(0)+-}_{i\alpha} I_\alpha \sum_\beta [\delta_{\alpha\beta} - I_\beta\chi^{(0)+-}_{\alpha\beta}]^{-1}\chi^{(0)+-}_{\beta j}, \quad (4)$$

where $\tilde{\chi}^{(0)+-}_{ij}$ corresponds to the Fe-Fe bare susceptibility enhanced by interaction with the Rh/Ru sublattice. In general, $[\delta_{\alpha\beta}-I_\beta\tilde{\chi}^{(0)+-}_{\alpha\beta}]$ represents a two-dimensional matrix in real space as can be seen from our results for J_{ij} listed in Table II. $\chi^{(0)+-}_{\alpha\beta}$ values decrease rapidly with increasing Rh/Ru-Rh/Ru distance and the on-site susceptibility gives its primary contribution. Therefore, the matrix will be diagonal and using the reduced expression for the exchange parameters, $\tilde{J}_{ij}=-\Delta_i\tilde{\chi}^{(0)+-}_{ij}\Delta_j$, we obtain the final expression for Fe-Fe exchange coupling to be

$$\tilde{J}_{ij} = J_{ij} + \sum_\alpha J_{i\alpha}\frac{(I_\alpha/\Delta^2_\alpha)}{1-(I_\alpha/\Delta^2_\alpha)J_{\alpha\alpha}}J_{\alpha j}, \quad (5)$$

where J_{ij} and $J_{i\alpha}$ are, respectively, Fe-Fe and Fe-Rh/Ru exchange couplings calculated before enhancement; $J_{\alpha\alpha}$ is the on-site Rh/Ru exchange coupling.

Interactions between the magnetic moment of atom i and the magnetic moments of all other atoms determine the effective exchange parameter at atom i, $(J_0)_i=\Sigma'_j J_{ij}$. $(J_0)_i$ also equals the second derivative of the total energy relative to angular deviations from an initially collinear configuration of magnetic moments, i.e., $(J_0)_i=\partial^2 E/\partial\theta^2_i$, with respect to either ferromagnetic (FM) or antiferromagnetic (AFM) arrangements of magnetic moments. From this perspective, $(J_0)_i$ will be positive valued for the stable magnetic state and negative valued for the unstable one.

The exchange parameters J_{ij} (model 1) or $\tilde{J}_{ij}$ (model 2) are used for the calculation of transition temperatures T_C or T_N in the mean-field approximation as a largest solution of the equation

$$\det\left(\frac{2}{3}(J_0)_{nm} - T\delta_{nm}\right) = 0, \quad (6)$$

where n and m are the indices of the inequivalent magnetic sublattices, and $(J_0)_{nm}$ is an effective exchange interaction between one atom from sublattice n with all atoms from sublattice m,[28,29] i.e., $(J_0)_{im}=\Sigma'_{j\in m}J_{ij}$ (or $\tilde{J}_{ij}$), for a summation over all atoms j in the magnetic sublattice m.

To investigate the dimensionality of the magnetic system in $Sc_2Fe(Ru_{1-x}Rh_x)_5B_2$, spin wave dispersion curves, $\omega_\nu(\mathbf{k})$, were calculated.[30] This result can be confirmed by inelastic neutron scattering experiments. The expression for the calculation of $\omega_\nu(\mathbf{k})$ from the calculated J_{ij} parameters is described in Appendix B.

III. RESULTS AND DISCUSSION

A. bcc 3*d* metals

We start our analysis with nonmagnetic, bcc iron and the 3*d* series of the magnetic elements. The COHP curve for the nearest neighbor interactions as a function of the number of *d* electrons (see Ref. 31 for more details), as well as the effective total exchange parameter J_0 as a function of the band filling, is presented in Fig. 2 (in this case, there is a single effective exchange parameter). These figures are based on a self-consistent calculation of bcc-Fe itself, where the change in the valence electron number N is introduced solely by a rigid-band approach.

A systematic change occurs in the nearest neighbor COHP and J_0 as a function of the *d* band filling.[25] Whenever the number of valence electrons per atom is smaller than 7.5, such as in manganese or chromium, the FM state is no longer stable ($J_0<0$). This result agrees well with experiment and also correlates with the nearest neighbor COHP interpretation [ferromagnetism for the Fermi level (E_F) positioned in antibonding states, and antiferromagnetism when E_F is located among nonbonding states]. Thus, the COHP interpretation identifies chromium as an ideal antiferromagnet where E_F exactly separates bonding states from antibonding states.

To demonstrate the general character of this result, we calculated the variation of J_0 with band filling for a model rectangular density of states (DOS; see Fig. 3]. For such a DOS, all potential parameters, except the center of the band

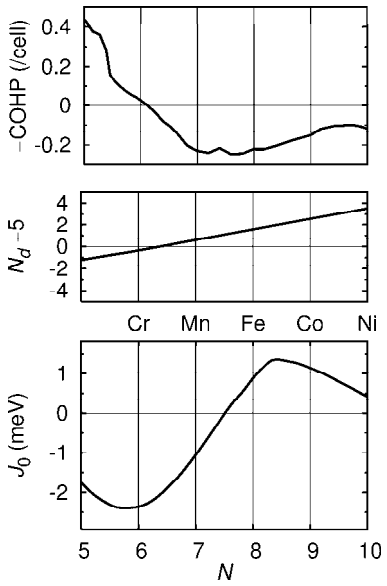

FIG. 2. (Top) Variation of $M-M$ bonding in the series of bcc $3d$ transition metals based on a COHP analysis of Fe–Fe bonding in nonmagnetic bcc Fe assuming a rigid-band behavior; the COHP is shown as a function of the number of the valence electrons N. (Middle) The occupation of the $3d$ states as a function of N in nonmagnetic bcc Fe. (Bottom) The effective exchange coupling parameter as a function of N in bcc Fe based on the FM state.

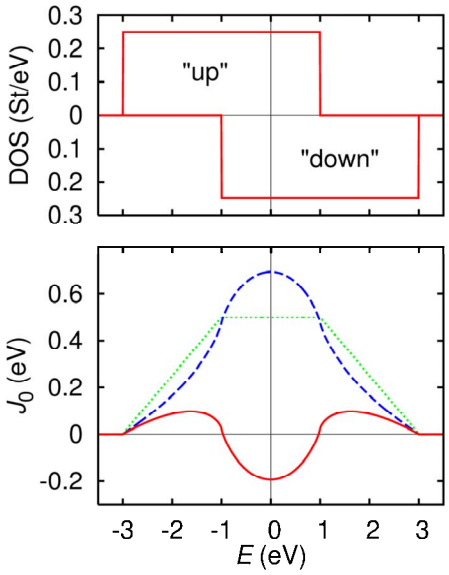

FIG. 3. (Color online) Rectangular DOS curves for spin "up" and spin "down" bands. (Bottom) Effective exchange parameter $(J_0)(E_F)$ as a function of band filling (red-solid curve) based on the rectangular DOS. The first, $\Delta_l\, M_l(E_F)$, and second, $\Delta_l\, \chi_{ll}^{+-}(E_F)\, \Delta_l$, contributions to $(J_0)(E_F)$ are shown, respectively, in green dotted and blue dashed. See text for further details.

(C_l^σ), are equal for spin up and down. In this case the expression for J_0 [see Eq. (A5) in Appendix A] can be reduced to the form[25]

$$J_0(E_F) = \frac{1}{2\pi}\int^{E_F} d\varepsilon\ \mathrm{Im} \sum_{L,L'} [\Delta_l(G_{L;L}^{\uparrow} - G_{L;L}^{\downarrow}) + 2\Delta_l G_{L;L'}^{\uparrow}\Delta_{l'} G_{L';L}^{\downarrow}], \tag{7}$$

where $\Delta_l = (C_l^{\uparrow} - C_l^{\downarrow})/2$ is the splitting between spin up and down bands and $G_{L;L'}^{\sigma}(\varepsilon)$ is the usual Green's function for spin σ and a single site in the unit cell

$$G_{L;L'}^{\sigma}(\varepsilon) = \sum_{\nu} \int \frac{d\mathbf{k}}{\Omega_{BZ}} \frac{X_{\nu,L}^{\sigma}(\mathbf{k})[X_{\nu,L'}^{\sigma}(\mathbf{k})]^*}{\varepsilon - \varepsilon_{\nu}^{\sigma}(\mathbf{k})}, \tag{8}$$

where $X_{\nu,L}^{\sigma}(\mathbf{k})$ and $\varepsilon_{\nu}^{\sigma}(\mathbf{k})$ are, respectively, the eigenvectors and eigenvalues of the Schrödinger equation. Using the relationship between the Green's function and the partial density of states, $N_L^{\sigma}(\varepsilon) = -\frac{1}{\pi}\,\mathrm{Im}\, G_{L;L}^{\sigma}(\varepsilon + i0)$, Eq. (7) can be reduced to the form

$$J_0(E_F) = \Delta_l M_l(E_F) - 2\Delta_l \chi_{ll}^{+-}(E_F)\Delta_l, \tag{9}$$

where $M_l(E_F)$ is the magnetic moment for E_F corresponding to the l band and $\chi_{ll}^{+-}(E_F)$ is the corresponding static transverse susceptibility. The first contribution to $J_0(E_F)$ $\Delta_l \cdot M_l(E_F)$, shown by the dotted green line in the lower graph of Fig. 3, linearly increases from the bottom of the spin up band at −3 eV to the bottom of the spin down band at −1 eV, then remains constant to the top of the spin up band at +1 eV (between −1 and +1 eV, the difference between the spin up and spin down partial DOS is zero), and finally linearly decreases to zero at the top of the spin down band at +3 eV. The second contribution, $2\Delta_l \chi_{ll}^{+-}(E_F)\Delta_l$, shown by the dashed blue line, is the "self-exchange" term. This analysis indicates that $\Delta_l M_l(E_F)$ exceeds $2\Delta_l \chi_{ll}^{+-}(E_F)\Delta_l$ near the bottom and top of this rectangular DOS, but that $2\Delta_l \chi_{ll}^{+-}(E_F)\Delta_l$ exceeds $\Delta_l M_l(E_F)$ around the middle of the band. The two terms are exactly equal at the partial spin up and spin down DOS boundaries. When $J_0(E_F) > 0$ (for -3 eV $< E_F < -1$ eV and $+1$ eV $< E_F < +3$ eV), FM ordering is stable, whereas for $J_0(E_F) < 0$ (for -1 eV $< E_F < +1$ eV), AFM ordering is stable. Therefore, the ground state of a system with a nearly empty or filled band is FM, and AFM for nearly half filled. In this model, we did not use any information about the band's character, i.e., crystal structure effects or specific atomic orbitals, e.g., d states. Nevertheless, regions of the DOS near band centers are generally nonbonding; strong bonding or antibonding interactions occur, respectively, at the lower and upper bounds of the DOS. Furthermore, the Stoner criterion must be satisfied for the existence of the magnetic state.

Variation in $J_0(E_F)$ with respect to band filling from the t_{2g} bands in the bcc $3d$ metals (using Fe for the calculation) is similar to the rectangular band picture, as shown in Fig. 4; the variation in $J_0(E_F)$ from the e_g states is close to the t_{2g} curve. In general, the picture for bcc transition metals is close to the result presented for the model calculation, but there are some differences in the shape of the $J_0(E_F)$ curve determined by the differences in shapes of the respective DOS curves.

B. $Sc_2Fe(Ru_{1-x}Rh_x)_5B_2$

The numerical results for the entire $Sc_2Fe(Ru_{1-x}Rh_x)_5B_2$ series are presented in Tables I and II, which summarize the

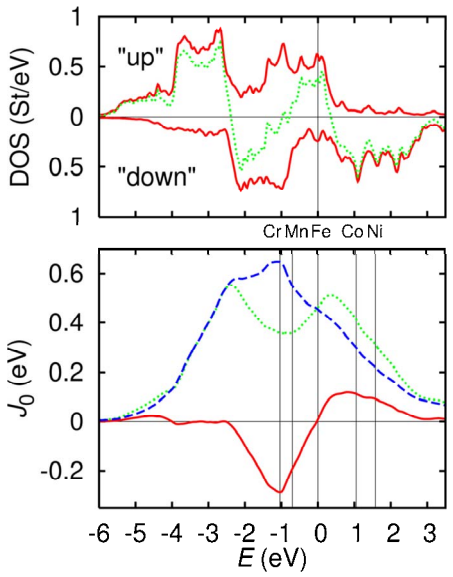

FIG. 4. (Color online) (Top) t_{2g} DOS (spin "up" and spin "down" curves are red; the difference curve is green) and (bottom) t_{2g} contribution to the effective exchange parameter J_0 as a function of band filling for bcc $3d$ transition metals (red-solid curve). The first, $\Delta_l M_l(E_F)$, and second, $\Delta_l \chi_{ll}^{+-}(E_F)\ \Delta_l$, contributions to J_0 are shown, respectively, in green dotted and blue dashed. Band filling in the rigid-band approximation for Cr, Mn, Fe, Co, and Ni are indicated on the bottom graph.

calculated values of the local magnetic moments, the total energy differences between the FM and AFM states, the effective exchange parameters, as well as the ordering temperatures. The magnetic moments on the Sc, Rh1, and B atoms are negligibly small and are not included in the table.

For $Sc_2FeRh_5B_2$ ($x=1$), the calculated Fe magnetic moment equals $3.4\mu_B$ using the LSDA approach ($3.5\mu_B$ with the GGA), which is much larger than in bcc Fe ($2.2\mu_B$). Due to strong mixing between the Fe $3d$ orbitals with the $4d$ orbitals of the eight nearest Rh2 neighbors, a significant spin polarization at the Rh2 atoms ($0.25\mu_B$ in LSDA; 0.27 in GGA) results (see partial DOS shown in Fig. 5). This polarization is also reflected in nonzero $(J_0)_{\mathrm{Rh2}}$ values of 11 meV. For comparison, the $(J_0)_{\mathrm{Fe}}$ value corresponds to 65 meV. In general, the GGA gives larger magnetic moments compared to LSDA results, which is similar to results for bulk $3d$ magnetic metals Fe, Co, and Ni,[32] as well as larger exchange parameters −12 and 79 meV, correspondingly, for $(J_0)_{\mathrm{Rh2}}$ and $(J_0)_{\mathrm{Fe}}$. Upon reducing the number of valence electrons on going from $Sc_2FeRh_5B_2$ (65 electrons) to $Sc_2FeRu_5B_2$ (60 electrons), all moments and exchange parameters become smaller. The T_C or T_N ordering temperatures were calculated according to the MFA (in the system with two magnetic atoms per cell) using Eq. (6); the corresponding effective exchange interactions for the different sublattices $(J_0)_{mn}$, which are used in Eq. (6), are listed in Table II. The theoretical Curie temperature T_C of $Sc_2FeRh_5B_2$ obtained from LSDA exchange parameters equals 270 K, a value which underestimates the experimental result[33] by nearly 200 K; the GGA result is 335 K and remains significantly smaller than the experimental value. The results in Table I also reflect the usual underestimation of the Curie temperatures for the entire series, just as for the related class of full Heusler alloys.[15]

As we mentioned in the first two sections, the model of rigid spins at Rh/Ru sites in systems related to the $Sc_2Fe(Ru_{1-x}Rh_x)_5B_2$ series is limited. To compare our initial MFA results, we used the effective spin Hamiltonian model,[7,8] in which rigid moments are assigned to Fe atoms only, moments which interact through effective exchange parameters, $\tilde{J}_{ij}=J_{ij}+(\frac{1}{2}I_\alpha\chi_\alpha^2)\Sigma_\alpha J_{i\alpha}J_{\alpha j}$, where J_{ij} is the bare Fe-Fe exchange interaction, I_α is the Stoner parameter for Ru or Rh, χ_α is the Rh/Ru longitudinal susceptibility, $\sim 4\times 10^{-4}$ meV^{-1} (estimated from the Rh/Ru partial density of states at the Fermi energy), and index α corresponds to Rh/Ru atoms. The coefficient in front of the summation over α, $(\frac{1}{2}I_\alpha\chi_\alpha^2)$ in the expression for $\tilde{J}_{ij}$, is 6×10^{-5} meV^{-1}, a value which suppresses the contributions from Fe-Rh/Ru interactions to $\tilde{J}_{ij}$ in the $Sc_2Fe(Ru_{1-x}Rh_x)_5B_2$ family of compounds. As a result, T_C obtained from this effective Heisenberg model is even smaller compared to a rigid Rh/Ru spin model. Results in better agreement with experiment come from model 2. The enhancement produced by the Rh/Ru magnetic subsystem increases $(J_0)_{\mathrm{Fe\text{-}Fe}}$ to 57 meV and the subsequent MFA result for T_C is 440 K; the corresponding CVM result is 350 K. For systems with small numbers of nearest neighbors, Curie temperatures predicted by the MFA typically exceed those calculated by other, more accurate models, e.g., CVM or Monte Carlo.[17] Although models 1 and 2 underestimate the experimental Curie temperature (~450 K), model 2 is a distinct improvement through the enhancement of the Rh/Ru subsystem. Higher accuracy cannot be achieved using the proposed formalism.

The DOS plot of $Sc_2FeRh_5B_2$ together with the partial DOS curves (LSDA result) is presented in Fig. 5. The $3s$ states of the boron atoms occur between −10.9 and −8.2 eV and are separated from the conduction band by a 1.4 eV gap. Figure 5 also indicates larger magnetic polarization of the Rh2 sites as compared to the Rh1 atoms around the Fermi energy, an effect which is induced by Fe atoms. Preference for the FM ground state of $Sc_2FeRh_5B_2$ ($x=1$) can also be extracted from the numerical results listed in Table I; the AFM state lies higher in energy by 536 K in LSDA (631 K in GGA), but IS STABLE with respect to small fluctuations of the direction of the spin moment, i.e., $(J_0)_{\mathrm{Fe}}^{(\mathrm{AFM})}$, $(J_0)_{\mathrm{Rh2}}^{(\mathrm{AFM})} > 0$. In such a case, it is possible to find metamagnetic transitions from a FM state at low temperature to an AFM state at a somewhat higher temperature, and then to the paramagnetic state.[1,2]

Figure 6 illustrates the course of the effective exchange parameters $(J_0)_{\mathrm{Fe}}^{(\mathrm{FM})}$ as a function of the band energy for the phases $Sc_2FeRh_5B_2$ ($x=1$) and $Sc_2FeRu_5B_2$ ($x=0$) calculated in LSDA using model 1. The GGA does not change our results significantly and model 1 provides a relevant description of the stability of FM and AFM orders. Figure 6 also shows the partial DOS of the Fe and Rh2 (or Ru2) atoms in the two compounds. Clearly, these curves are quite similar in shape but not in magnitude, and the different valence electron counts (depicted as solid and dashed Fermi levels in Fig.

TABLE I. Calculated and experimental results for $Sc_2Fe(Ru_{1-x}Rh_x)_5B_2$ ($0 \leqslant x \leqslant 1$): (i) the total energy difference ΔE (K/unit cell) between the FM and AFM ordered states ($\Delta E = E_{FM} - E_{AFM}$), (ii) local magnetic moments (μ_B), and effective exchange parameters (meV) for Fe ($2\times$) and Rh2 ($8\times$) sites in FM and AFM ordered (MO) states; and (iii) ordering temperatures, T_C or T_N (K), calculated in the MFA using LSDA and GGA, compared with the experimental values (Expt.) and values obtained by "model 2 (M2)," in which we add Rh/Ru enhancement to Fe exchange parameters. The labels "unst" in the MFA columns means that the corresponding magnetic ordering is unstable, i.e., $(J_0)_i < 0$; "—" in the Expt. column indicates this type of ordering is not observed experimentally. The Néel temperature for $x = 0.4$ is not known.

x	ΔE (K)				μ_B		T_C or T_N (K)			
(N)	LSDA	GGA	MO	Class	LSDA	GGA	LSDA	GGA	M2	Expt.[a]
1.0	−536	−631	FM	Fe	3.42	3.47	270	335	440	≈450
(65)	(FM)	(FM)		Rh2	0.25	0.27				
			AFM	Fe	±3.41	±3.48	193	237	230	—
				Rh2	±0.18	±0.19				
0.8	−562	−694	FM	Fe	3.36	3.43	220	265	356	≈350
(64)	(FM)	(FM)		Rh2/Ru2	0.22	0.23				
			AFM	Fe	±3.38	±3.45	113	141	113	—
				Rh2/Ru2	±0.19	±0.19				
0.6	185	142	FM	Fe	3.16	3.27	103	165	187	≈300
(63)	(AFM)	(AFM)		Rh2/Ru2	0.15	0.17				
			AFM	Fe	±3.18	±3.29	160	195	204	—
				Rh2/Ru2	±0.16	±0.16				
0.4	1090	1168	FM	Fe	2.96	3.09	unst	34	71	—
(62)	(AFM)	(AFM)		Rh2/Ru2	0.08	0.08				
			AFM	Fe	±3.01	±3.14	173	266	320	—
				Rh2/Ru2	±0.11	±0.10				
0.2	21	−221	FM	Fe	2.74	2.90	unst	14	37	—
(61)	(AFM)	(FM)		Rh2/Ru2	−0.02	−0.03				
			AFM	Fe	±2.77	±2.92	5	55	278	≈10
				Rh2/Ru2	±0.04	±0.04				
0.0	257	47	FM	Fe	2.69	2.84	unst	unst	unst	—
(60)	(AFM)	(AFM)		Ru2	−0.08	−0.03				
			AFM	Fe	±2.70	±2.87	116	148	378	≈13
				Ru2	±0.04	±0.04				

[a]Reference 24.

6) make $Sc_2FeRh_5B_2$ a ferromagnet and $Sc_2FeRu_5B_2$ an antiferromagnet. The crossover between FM and AFM ordering is reached at a valence electron count of 63 electrons; below this number, AFM ordering is preferred. The same result can also be inferred from Fig. 7, which shows the variations of $(J_0)_{Fe}^{(FM)}$ and $(J_0)_{Fe}^{(AFM)}$ as a function of the valence electron count, and is in perfect agreement with the COHP picture.[5] Figure 7 (middle) directly displays the energy difference between the FM ($N=64$ or 65 electrons) and the AFM ($N=60-63$ electrons) states.

As we have already mentioned, the pair exchange interactions J_{ij} are not entirely localized between the Fe atoms (see Table II), despite the fact that the largest J_{ij} values correspond to the interactions of two nearest Fe neighbors and are, respectively, 10 and 1.6 meV in LSDA (13 and 0.5 meV in GGA). Exchange interactions between different Fe chains (entries 3 and 5 in Table II) are almost zero such that the chemical picture of almost isolated one-dimensional (1D) Fe chains (see Fig. 1, left) seems, at first glance, justified. Nonetheless, there are significant Fe-Rh2 exchange interactions, which may be understood from the relatively large spin polarization induced on Rh2 sites because of the short Fe-Rh2 distance. In fact, the total contribution from the eight neighboring Rh2 atoms to the effective exchange parameter $(J_0)_{Fe}$ is larger than the bare Fe-Fe contribution.

The chemical picture of almost isolated 1D Fe chains raises a very important question about whether this system should be discussed as a 1D magnetic system. This question is important because of the fact that a 1D magnetic chain described by an isotropic classical Heisenberg model does not have long range order at any temperature.[34] An answer could be obtained from magnon dispersion curves, $\omega_\nu(\mathbf{k})$. In

TABLE II. Pairwise exchange parameters J_{ij} (meV) for Fe-X pairs (index i=Fe), R/a being the relative interatomic distance, $[R_x/a, R_y/a, R_z/c]$ the corresponding vector, M is the number of equivalent pairs, and $(J_0)_{im}$ is the effective exchange parameters. M1 = "model 1," M2 = "model 2."

						J_{ij}						$(J_0)_{im}$					
						FM			AFM			FM			AFM		
x		X in				M1		M2	M1		M2	M1		M2	M1		M2
(N)		Fe-X	R/a	$[R_x/a, R_y/a, R_z/c]$	M	LDA	GGA	GGA	LDA	GGA	GGA	LDA	GGA	GGA	LDA	GGA	GGA
1.0	1	Fe	0.331	[0,0,1]	2	10.00	13.04	20.75	11.76	13.95	16.73	22.7	26.6	43.8	44.4	17.7	27.3
(65)	2	Fe	0.661	[0,0,2]	2	1.62	0.45	2.06	0.39	0.68	1.64						
	4	Fe	0.992	[0,0,3]	2	0.38	0.80	0.91	1.06	1.52	1.58						
	5	Fe	1.000	[0,1,0]	4	−0.03	0.11	0.11	0.11	−0.05	−0.05						
	3	Fe	0.707	[1/2,1/2,0]	4	0.18	−0.15	0.49	−1.13	−0.82	−1.22	0.3	4.2	13.3	−24.8	6.9	2.3
	6	Rh	0.282	[0.22,−0.07,1/2]	8	3.77	4.34		2.92	3.33		35.6	41.0		27.4	30.8	
	7	Rh	0.540	[0.43,−0.28,1/2]	8	0.44	0.46		−0.37	−0.38		5.3	5.6		−4.3	−3.7	
0.8	1	Fe	0.331	[0,0,1]	2	6.58	9.22	15.51	4.23	7.64	10.67	16.2	19.9	36.5	15.5	38.4	50.00
(64)	2	Fe	0.661	[0,0,2]	2	2.03	1.00	2.59	3.07	3.79	4.85						
	4	Fe	0.992	[0,0,3]	2	1.20	1.65	1.77	1.20	1.97	2.05						
	5	Fe	1.000	[0,1,0]	4	−0.14	−0.22	−0.22	−0.18	−0.25	−0.25						
	3	Fe	0.707	[1/2,1/2,0]	4	−0.53	−0.64	−0.12	−1.01	−1.35	−1.68	1.5	2.7	9.6	−10.3	−29.9	−35.4
	6	Rh	0.282	[0.22,−0.07,1/2]	8	3.20	3.69		2.67	3.02		31.7	36.2		26.4	30.3	
	7	Rh	0.540	[0.43,−0.28,1/2]	8	0.30	0.34		−0.26	−0.27		3.3	3.8		−2.9	−3.6	
0.6	1	Fe	0.323	[0,0,1]	2	12.28	15.91	18.18	7.34	9.07	10.55	20.1	27.9	32.1	9.2	11.9	14.6
(63)	2	Fe	0.646	[0,0,2]	2	−4.46	−3.93	−3.63	−3.10	−2.31	−2.09						
	4	Fe	0.969	[0,0,3]	2	0.64	0.08	0.09	1.65	1.85	1.86						
	5	Fe	1.000	[0,1,0]	4	0.72	0.88	0.88	0.08	0.18	0.18						
	3	Fe	0.707	[1/2,1/2,0]	4	−2.92	−2.58	−2.43	3.40	3.33	3.22	−8.7	−8.6	−7.9	11.0	12.5	11.8
	6	Rh/Ru	0.278	[0.22,−0.07,1/2]	8	1.17	1.46		0.92	1.17		9.5	12.0		7.5	9.6	
	7	Rh/Ru	0.540	[0.43,−0.28,1/2]	8	0.10	0.11		−0.08	−0.10		0.8	1.0		−0.3	−0.6	
0.4	1	Fe	0.323	[0,0,1]	2	4.60	6.94	12.41	2.07	6.84	11.03	2.6	15.6	25.8	1.3	10.5	18.0
(62)	2	Fe	0.646	[0,0,2]	2	−6.27	−4.02	−3.07	−3.92	−3.58	−3.01						
	4	Fe	0.969	[0,0,3]	2	1.94	3.14	3.19	1.41	0.16	0.18						
	5	Fe	1.000	[0,1,0]	4	−0.11	−0.01	−0.01	0.00	0.03	0.03						
	3	Fe	0.707	[1/2,1/2,0]	4	−5.05	−4.28	−4.28	4.95	5.25	5.25	−16.3	−16.6	−16.6	20.6	23.3	23.3
	6	Rh/Ru	0.278	[0.22,−0.07,1/2]	8	0.73	1.14		0.86	1.02		6.2	9.7		7.1	8.3	
	7	Rh/Ru	0.540	[0.43,−0.29,1/2]	8	0.00	0.00		0.00	0.00		0.0	0.0		0.0	0.0	
0.2	1	Fe	0.323	[0,0,1]	2	2.86	5.71	6.58	8.47	10.76	20.20	−0.1	5.0	6.9	−6.8	−4.5	12.5
(61)	2	Fe	0.646	[0,0,2]	2	−4.41	−4.09	−4.23	−6.68	−6.05	−6.58						
	4	Fe	0.969	[0,0,3]	2	−0.34	−0.73	−0.72	−3.69	−3.92	−3.91						
	5	Fe	1.000	[0,1,0]	4	0.30	0.23	0.23	0.18	0.27	0.27						
	3	Fe	0.707	[1/2,1/2,0]	4	0.14	−0.10	−0.03	0.80	1.13	2.2	−2.2	−3.4	−2.1	5.0	11.3	23.5
	6	Ru	0.278	[0.22,−0.07,1/2]	8	0.04	0.10		0.32	0.37		0.4	0.9		2.1	2.7	
	7	Rh	0.540	[0.43,−0.29,1/2]	8	0.01	0.01		0.04	0.04		0.1	0.16		0.4	0.5	
0.0	1	Fe	0.323	[0,0,1]	2	1.07	3.51	4.85	4.26	6.94	13.77	−1.6	2.3	2.3	−0.2	6.6	19.9
(60)	2	Fe	0.646	[0,0,2]	2	−3.21	−3.94	−3.47	−2.76	−3.29	−3.40						
	4	Fe	0.969	[0,0,3]	2	0.42	0.20	0.66	−1.94	−2.48	−2.36						
	5	Fe	1.000	[0,1,0]	4	0.18	0.19	0.19	0.29	0.34	0.34						
	3	Fe	0.707	[1/2,1/2,0]	4	−1.17	−1.32	−1.24	1.63	1.64	2.14	−12.5	−14.6	−14.6	15.1	12.4	29.0
	6	Ru	0.278	[0.22,−0.07,1/2]	8	0.07	0.11		0.27	0.35		0.7	1.1		1.8	2.3	
	7	Ru	0.540	[0.43,−0.29,1/2]	8	0.01	0.01		0.03	0.02		0.1	0.1		0.7	0.8	

a 1D magnetic system, $\omega_\nu(\mathbf{k})$ should be constant along any direction in planes perpendicular to the direction of the chain. $\omega_\nu(\mathbf{k})$ curves for $Sc_2FeRh_5B_2$, shown in Fig. 8, were calculated using Eq. (B1) in Appendix B and the theoretical J_{ij} values from Table II. The strongest dispersions, ~100 meV, occur along the Γ-Z and A-M directions, which are parallel to the 1D Fe chains; there are also significant dispersions, ~25 meV, along both the Γ-X and Γ-M directions, which are perpendicular to these chains. Such dispersion cannot be presented in strictly 1D magnetic systems.

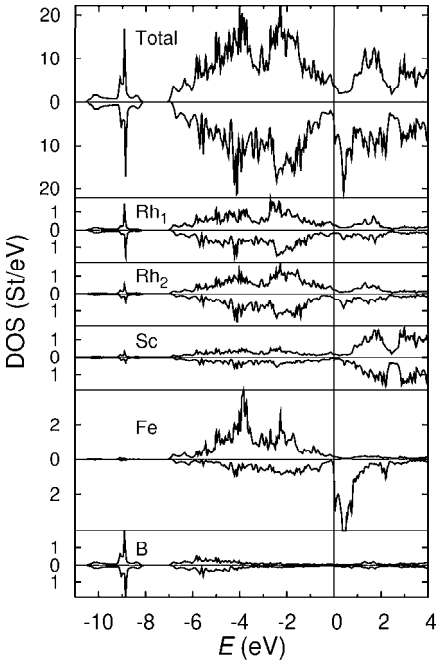

FIG. 5. Total and partial DOS curves in FM $Sc_2FeRh_5B_2$. The Fermi level corresponds to the energy zero. The total DOS is presented in states/eV cell, whereas partial DOS curves are presented in states/eV atom.

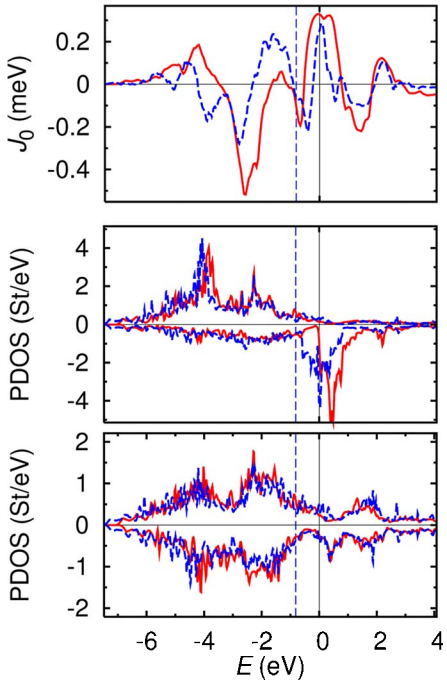

FIG. 6. (Color online) (Top) The effective exchange constant $(J_0)_{Fe}$ as a function of band filling in $Sc_2FeRh_5B_2$ (65 valence electrons, in red solid) and in $Sc_2FeRu_5B_2$ (60 valence electrons, in blue dashed). (Middle and bottom) The partial DOS curves, respectively, for Fe and Ru/Rh sites. The Fermi levels are shown by vertical lines, with the zero energy corresponding to an occupation number of 65 valence electrons.

The other interesting "feature" of the calculated $\omega_\nu(\mathbf{k})$ curves is the existence of an optical mode located around 170 meV. This branch of the magnon spectrum is determined by fast oscillations of the small magnetic moments at Rh2 sites in the field produced by interaction with Fe atoms.

In model 2, all interactions J_{ij} are localized between Fe sites. The presence of Rh/Ru atoms both enhances Fe-Fe exchange interactions within chains up to 21 and 2 meV and produces sizable interactions ($\sim$0.5 meV) between chains. Since there are only two magnetic atoms in the unit cell in model 2, $\omega_\nu(\mathbf{k})$ curves (Fig. 8) have only two branches but the dispersion in directions perpendicular to the Fe chains is significant. This dispersion is determined by exchange couplings J_3 and J_5, which are almost 20 times smaller than intra-chain coupling J_1 (see Table II) for $Sc_2FeRh_5B_2$ ($x=1.0$). A similarly small in-plane dispersion should be expected in the FM-ordered compound with $x=0.8$. However, for lower values of x and AFM ordering, these exchange interactions are much larger, and we anticipate larger in-plane dispersion of these magnon waves. Since $\omega_\nu(\mathbf{k})$ are determined by the poles of the dynamic transverse magnetic susceptibility $\chi^{+-}(\mathbf{k},\omega)$, to verify the applicability of both approximations, more accurate calculations of $\omega_\nu(\mathbf{k})$ from $\chi^{+-}(\mathbf{k},\omega)$ need to be done. For the purpose of estimating the values of the pairwise exchange interactions J_{ij} in a compound with 62 valence electrons, we used the electronic structure results of the compound with 65 valence electrons and calculated the integral in expression (2) up to an E_F value that gives the occupation of rigid bands to be 62 electrons. The largest J_{ij} values (−9 meV in LSDA) calculated by this approach are negative and correspond to interactions between two Fe atoms in the unit cell related to the vector $(a/2)(\mathbf{x}+\mathbf{y})$ (entry 3 in Table II). From this result, a possible ground state for this spin system is AFM with the magnetic moments of the two chains of Fe atoms along the c direction in the unit cell aligned along opposite directions.

To check the applicability of the rigid-band approximation, we also calculated $(J_0)_{Fe}$ as a function of the band energy for $Sc_2FeRu_5B_2$ and placed it on the same plot with the calculated results of $Sc_2FeRh_5B_2$ (see again Fig. 7). The two curves show the same general tendencies with qualitative similarities. Any numerical discrepancies are almost exclusively related to the $\sim$20% larger bandwidth of the Ru $4d$ band compared to the Rh $4d$ band. This well-known phenomenon, which is readily apparent from the DOS curves of elemental fcc Ru and fcc Rh, but using the lattice parameter for Ru, can be attributed to the larger effective nuclear charge of Rh over Ru and the corresponding greater orbital overlaps between Ru atoms than between Rh atoms.

An impressive example of the influence of Ru/Rh substitution on physical properties occurs in the perovskitelike phases $CaRu_{1-x}Rh_xO_3$.[35] Low doping levels of Rh for Ru into this phase effectively narrows the $4d$ band and enhances the spin correlation. This effect triggers a metal-insulator transition and alters the spin coupling, thereby giving rise to a magnetically ordered phase. In our $Sc_2Fe(Ru_{1-x}Rh_x)_5B_2$ case, the substitution of Rh by Ru leads to a significant reduction of the spin moment at the Fe atoms, namely, from $3.42\mu_B$ to $2.70\mu_B$. For the other magnetically active atoms, the corresponding change is from $0.25\mu_B$ at Rh to $-0.08\mu_B$ at Ru. Such a reduction of the magnetic characteristics siz-

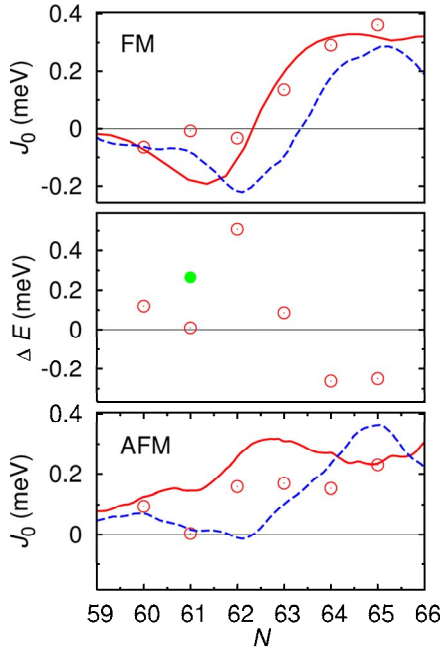

FIG. 7. (Color online) The effective exchange constant $(J_0)_{Fe}$ as a function of valence electron count (N) calculated for $Sc_2FeRh_5B_2$ (in red solid) and $Sc_2FeRu_5B_2$ (in blue dashed) assuming a rigid-band approximation for FM (top) and AFM (bottom). Individual points in the top/bottom figures correspond to exact calculated results as a function of N. (Middle) The total energy difference between FM and AFM ordering, $\Delta E = E_{FM} - E_{AFM}$. The green point identifies ΔE between the FM and AFM-2 magnetic structures (see text).

ably changes the Ru-Fe contribution to the effective exchange parameter $J_0)_{Fe}$ and its dependency on band filling.

Upon decreasing the concentration of Rh atoms, the ground state changes from FM to AFM at $x=0.6$ (or 63 valence electrons, see above) and below (see Fig. 7, middle). This result is independent of both LSDA and GGA approaches. The only exception occurs for $x=0.2$, where AFM ordering is stable for LSDA but FM for the GGA approach. However, we-shall demonstrate that AFM ordering is quite complicated at this concentration. Together with the change of the ground-state magnetic ordering with chemical composition, the orientations of the induced magnetic moments at

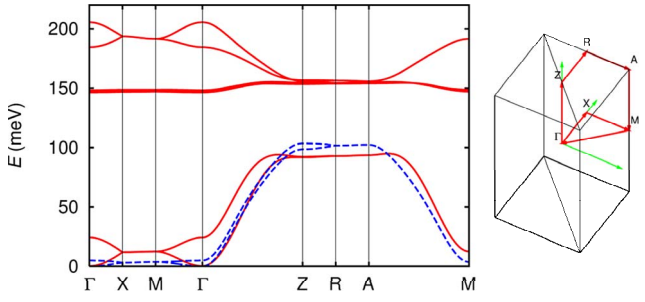

FIG. 8. (Color online) (Left) The calculated $\omega_\nu(\mathbf{k})$-magnon dispersion curves for $Sc_2FeRh_5B_2$ along specified directions in the irreducible wedge of the first Brillouin zone (right). Model 1 result is shown by red-solid and model 2 by blue-dashed lines.

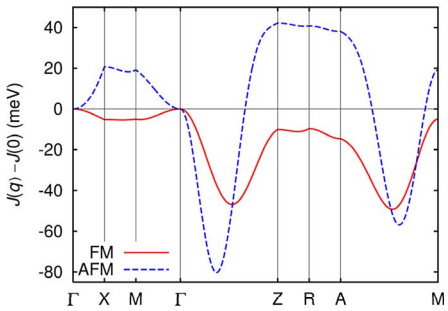

FIG. 9. (Color online) Fourier transform of the pairwise exchange parameters, J_{ij}, for FM (red solid) and AFM (blue dashed) $Sc_2FeRu_4RhB_2$ ($x=0.2$) along specified symmetry directions in the first Brillouin zone (see Fig. 9, right).

Rh (or Ru) also change their directions, from a parallel to an antiparallel orientation with respect to the Fe atoms (see spin moments in Table I). At $x \leqslant 0.2$, the effective exchange parameter $(J_0)_{Fe}$ of the FM state eventually becomes negative, and this type of spin ordering no longer corresponds to the local minimum. Also, the values of ΔE and (J_0)Fe in both the FM and AFM ordered states are small values at $x=0.2$. The zero value of $(J_0)_{Fe}$ is raised because of a significant compensation of nearest neighbor interactions by the next nearest neighbors (Table II). In such a "frustrated" system, more complicated types of magnetic ordering are likely, such as antiferromagnetism with large or even incommensurate ordering vectors. The classical ground state of the Heisenberg Hamiltonian (1) is known to be of the form $\mathbf{S}_i = \mathbf{u}\cos(\mathbf{Q}\cdot\mathbf{R}_i) + \mathbf{v}\sin(\mathbf{Q}\cdot\mathbf{R}_i)$,[36] where $\mathbf{u}$ and $\mathbf{v}$ are two orthonormal vectors, $\mathbf{R}_i$ is the position of site i in real space, and the wave vector $\mathbf{Q}$ has to minimize $J(\mathbf{q})$, which is the Fourier transform of the pairwise exchange parameters, $J(\mathbf{q}) = \Sigma_{i,j} J_{ij}\cos[\mathbf{q}\cdot(\mathbf{R}_i - \mathbf{R}_j)]$. For the cases of either FM or AFM ordering used to calculate the J_{ij} values, the wave vector $\mathbf{Q}$ should correspond to zero. As seen from the $J(\mathbf{q})$ variations along various symmetry directions in the Brillouin zone in Fig. 9, neither FM nor AFM ordering based on one unit cell satisfies this condition. The minima of $J(\mathbf{q})$ correspond to incommesurate spin structure with a characteristic wave vector $\mathbf{Q}$ $(2\pi/a)$ $[0,0,1/4(a/c)]$ and based on an AFM unit cell. This type of magnetic ordering was reproduced in the crystallographic unit cell by four unit cells repeated along the c direction (AFM-2). The magnetic moments of two Fe atoms in the two bottom cells are aligned in antiparallel directions. In the two top cells, magnetic moments are rotated by 180°. The excess energy of the AFM-2 state as compared to the FM state is shown by the green point in Fig. 7 for $N=61$ valence electrons.

Nonetheless, the ground state for $Sc_2FeRu_5B_2$ ($x=0$) is AFM ordered, and ΔE equals 257 K (47 K in GGA) in favor of antiferromagnetism. In contrast to $Sc_2FeRh_5B_2$ ($x=1$), FM ordering is unstable, $(J_0)\text{Fe} < 0$, while the $(J_0)_{Fe}$ value in the AFM-ordered phase is positive (17.4 meV in LSDA; 22 meV in GGA model 1, 49 meV in model 2). The Néel

TABLE III. Calculated pairwise exchange parameters J_{ij} (meV) for Fe-X pairs (index i=Fe), R/a being the relative interatomic distance, $[R_x/a, R_y/a, R_z/c]$ the corresponding vector, M is the number of equivalent pairs, $\Delta C(=C^{\uparrow}-C^{\downarrow})$ is the splitting between spin up and down $4d$ states of Rh/Ru atoms, $J_{\alpha\alpha}$ is on-site exchange parameter for Rh/Ru, and $\tilde{I}_{\alpha}$ is the renormalized Stoner exchange parameter used for calculation of enhanced Fe-Fe interactions as in Appendix C.

					J_{ij}						
					FM		AFM				
					M1		M1				
x (N)	Fe-X	R/a	$[R_x/a, R_y/a, R_z/c]$	M	LDA	GGA	LDA	GGA	ΔC	$J_{\alpha\alpha}$	$\tilde{I}_{\alpha}$
1.0 (65)	Rh	0.546	[0.22, −0.07, −3/2]	8	0.53	0.58	0.38	0.45	211	4.2	0.08
0.8 (64)	Rh	0.546	[0.22, −0.07, −3/2]	8	0.49	0.54	0.38	0.44	187	3.0	0.10
0.6 (63)	Rh/Ru	0.546	[0.22, −0.07, −3/2]	8	0.09	0.11	0.09	0.10	122	1.2	0.23
0.4 (62)	Rh/Ru	0.546	[0.22, −0.07, −3/2]	8	0.05	0.12	0.08	0.08	61	0.2	0.87
0.2 (61)	Ru	0.546	[0.22, −0.07, −3/2]	8	0.01	0.01	0.01	−0.01	10	−0.03	18
0.0 (60)	Ru	0.546	[0.22, −0.07, −3/2]	8	0.01	0.03	−0.04	−0.04	9	−0.03	18

temperatures calculated in mean-field approximation are, respectively, 116, 148, and 378 K. The CVM result for model 2 is 310 K. Again, in contrast to $x=0$, the theoretical values significantly overestimate experimental values of 13 K.

IV. CONCLUSIONS

For the entire homologous series $Sc_2Fe(Ru_{1-x}Rh_x)_5B_2$, magnetic measurements show a change from FM to AFM behavior as x decreases. The relationship between effective exchange coupling $(J_0)_i$ and COHP along the $3d$ series was investigated on a sample of bcc Fe. This analysis indicated the tendency for AFM ordering for nearly the half-filled band cases (Cr and Mn) and FM ordering for almost empty or almost filled band cases (Fe, Co, and Ni), and that this behavior correlates with the Fermi level falling, respectively, among metal-metal nonbonding or antibonding states. The general character of this trend was demonstrated on a calculation of $(J_0)_i$ using a model rectangular DOS. Using the same technique, the effective exchange interactions $(J_0)_i$ in $Sc_2Fe(Ru_{1-x}Rh_x)_5B_2$ followed a similar trend to $3d$ bcc metals as composition varies: $(J_0)_i$ takes negative values (AFM ordering) for low x with the Fermi level at metal-metal nonbonding states and changes to positive values (FM ordering) as x increases when the Fermi level falls at metal-metal antibonding states. Inclusion of gradient corrections to the local-spin-density approximation leads to larger magnetic moments and exchange interactions, but does not change this dependence. We propose a model in which Fe atomic moments are described by an independent rigid spin whereas interaction with the Rh/Ru magnetic sublattice leads to enhancement of Fe-Fe exchange. This description reproduces the Curie temperatures in much better agreement with experiment. Although transition temperatures are severely underestimated for FM phases and overestimated for AFM by both LSDA- and GGA-based models 1 and 2, the trends in magnetic ordering behavior are very well reproduced. The effective exchange couplings reveal significant Rh-Fe interactions that are the leading contributions to the FM coupling in the Rh-rich samples. In model 2, these interactions produce significant enhancement both within and between Fe chains. According to the calculation of spin wave dispersion, these Rh-Fe interactions eliminate 1D magnetic character for these materials. Furthermore, an incommesurate magnetic ordering along the c direction is predicted for a concentration $x=0.2$.

ACKNOWLEDGMENTS

One of the authors (G.D.S.) would like to thank N. E. Zein, O. N. Mryasov, and S. Blügel for helpful discussions. The authors acknowledge the generous financial support through a joint grant provided by the U.S. National Science Foundation (NSF DMR 05-02671) and the Deutsche Forschungsgemeinschaft (Germany).

APPENDIX A: CALCULATION OF PAIR AND EFFECTIVE EXCHANGE COUPLINGS

The pairwise exchange parameters J_{ij} are obtained by multiple scattering theory according to

$$J_{ij}=\frac{1}{2\pi}\int^{E_F} d\varepsilon\ \mathrm{Im}\sum_{L,L'}[\delta P_{i,l}(T^{\uparrow}_{i,L;j,L'}T^{\downarrow}_{j,L';i,L} + T^{\downarrow}_{i,L;j,L'}T^{\uparrow}_{j,L';i,L})\delta P_{j,l'}], \tag{A1}$$

where $\delta P(\varepsilon)_{i,l}=[P^{\uparrow}_{i,l}(\varepsilon)-P^{\downarrow}_{i,l}(\varepsilon)]/2$ is the on-site perturbation at atom i with orbital moment l, $P^{\sigma}_{i,l}(\varepsilon)$ is the potential function for site i with spin σ, $P^{\sigma}_{i,l}(\varepsilon)=[1/2(2l+1)][D^{\sigma}_{i,l}(\varepsilon)+l+1/D^{\sigma}_{i,l}(\varepsilon)-l]$, $D^{\sigma}_{i,l}(\varepsilon)$ is a wave function logarithmic derivative at the corresponding atomic sphere radius, and $T^{\sigma}_{iL,jL'}(\varepsilon)$ is the scattering-path operator connecting atoms i and j, dependent on the complex energy ε for the channel with spin σ ($\uparrow$ or $\downarrow$). L stands for (l,m), i.e., the orbital moment and its projection.[13]

The scattering-path operator for the complex energy ε is characterized in terms of the site-diagonal potential function P and the potential-independent structure constant S,

$$T^{\sigma}_{i,L;j,L'}(\varepsilon)=\int \frac{d\mathbf{k}}{\Omega_{BZ}} e^{i\mathbf{k}\cdot\mathbf{R}_{ij}}[P^{\sigma}_{i,l}(\varepsilon)-S_{i,L;j,L'}]^{-1}, \quad \text{(A2)}$$

where the integral is calculated over the irreducible wedge of the Brillouin zone and $\mathbf{R}_{ij}$ corresponds to the vector connecting atoms i and j. Note that $P(\varepsilon)$ is parametrized; the parametrization we employ corresponds closely to Anderson's third-order ASA Hamiltonian

$$P^{-1}(z)=\frac{\Delta}{C-z'}+\gamma-\alpha, \quad \text{(A3)}$$

with

$$z'=z+p(z-\varepsilon_{\nu})^3, \quad \text{(A4)}$$

where C, Δ γ, p, and ε_{ν} are standard LMTO parameters and α is the screening parameter.[37] For the calculation of the T matrix, we use the bare representation, in which the screening parameter $\alpha=0$.

Using the "sum rule," one may obtain[13] the expression for the effective ("on-site") exchange parameter to be

$$(J_0)_i=\sum_j{}' J_{ij}=\frac{1}{2\pi}\int^{E_F} d\varepsilon \,\mathrm{Im}\sum_{L,L'}[\delta P_{i,l}(T^{\uparrow}_{i,L;i,L}-T^{\downarrow}_{i,L;i,L}) + 2\delta P_{i,l}T^{\uparrow}_{i,L;i,L'}\delta P_{i,l'}T^{\downarrow}_{i,L';i,L}]. \quad \text{(A5)}$$

The above energy integrals in Eq. (A1) and (A5) were evaluated using a Gaussian quadrature with 12 points on an ellipse in the complex plane. Both the quadrature procedure and the number of $\mathbf{k}$ points in the Brillouin zone integral were carefully checked for their convergence properties.

APPENDIX B: EXPRESSION FOR SPIN WAVE DISPERSION IN THE SYSTEM WITH FEW ATOMS IN THE UNIT CELL

To obtain the magnon dispersion curves in the system with few magnetic atoms in the unit cell, we solved equation of motion for magnetic moments in the linear limit.[38] The spin wave dispersions, $\omega_{\nu}(\mathbf{k})$, where ν labels each band, are calculated as the eigenvalues of the system of linear equations

$$\sum_m \left[4(J_0)_n(\mathbf{0})\delta_{nm}-4\frac{M_n}{|M_n|}(J_0)_{nm}(\mathbf{k})-|M_n|\omega_{\nu}(\mathbf{k})\delta_{nm}\right]e_m(\mathbf{k},\nu)=0, \quad \text{(B1)}$$

where n and m are magnetic sublattices, M_n is the magnetic moment of atom n and $|M_n|$ is its absolute value, δ_{nm} is the Kronecker delta (1 for $n=m$; 0 for $n\neq m$), $e_m(\mathbf{k},\nu)$ is the eigenvector, and $(J_0)_{nm}(\mathbf{k})=\sqrt{2/N}\Sigma_{j\in m}J_{ij}e^{i\mathbf{k}\cdot(\mathbf{R}_i-\mathbf{R}_j)}$ with atom i from sublattice n, and $(J_0)_n(\mathbf{0})=\Sigma_m M_m/|M_m|(J_0)_{nm}(\mathbf{k}=\mathbf{0})$. This expression for $\omega_{\nu}(\mathbf{k})$ is equivalent to the earlier results from the Ref. 39. In contrast to the expressions from Ref. 39 however, we include the size of the magnetic moment ($|M_n|$) in the definition of J_{ij}.

APPENDIX C: EXPRESSION FOR RENORMALIZED EXCHANGE COUPLINGS

Following expression (5) for renormalized Fe-Fe pair exchange parameters, J_{ij} can be expressed as

$$\tilde{J}_1=J_1+4J_6\tilde{I}_{\alpha}J_6+4J_7\tilde{I}_{\alpha}J_7+2\times 4J_6\tilde{I}_{\alpha}J_8,$$

$$\tilde{J}_2=J_2+2\times 4J_6\tilde{I}_{\alpha}J_8,$$

$$\tilde{J}_3=J_3+4J_6\tilde{I}_{\alpha}J_7,$$

$$\tilde{J}_4=J_4+4J_8\tilde{I}_{\alpha}J_8,$$

$$\tilde{J}_5=J_5. \quad \text{(C1)}$$

The notation for J_i follows Table II; values for J_8 and $\tilde{I}_{\alpha}$ are listed in Table III.

The enhanced Rh/Ru Stoner exchange integral $\tilde{I}_{\alpha}$ was calculated from I_{α} (50 mRy) (Ref. 27) using the expression

$$\tilde{I}_{\alpha}=\frac{(4I_{\alpha}/\Delta C^2)}{1-(4I_{\alpha}/\Delta C^2)J_{\alpha\alpha}}. \quad \text{(C2)}$$

Finally, the expressions for renormalized effective Fe exchange couplings are

$$(\tilde{J}_0)_{11}=(J_0)_{11}+4(J_0)_{13}/4\tilde{I}_{\alpha}(J_0)_{13}/8+4(J_0)_{14}/4\tilde{I}_{\alpha}(J_0)_{14}/8,$$

$$(\tilde{J}_0)_{12}=(J_0)_{12}+4(J_0)_{13}/4\tilde{I}_{\alpha}(J_0)_{14}/4+4(J_0)_{14}/4\tilde{I}_{\alpha}(J_0)_{13}/4. \quad \text{(C3)}$$

There are two Fe atoms in the unit cell and index "11" corresponds to effective exchange coupling of the first Fe atom with all first atoms in other unit cells and index "12" for the first Fe with all second Fe atoms. The second index corresponds to number of line m of $(J_0)_{nm}$ as it presented in Table II. The coefficient 1/4 in expression (C3) arises because tabulated values include fourfold degeneracy; 1/8 corresponds to the usual 1/4 factor times an additional 1/2 to exclude self-interactions between Fe moments.

[1] E. A. Nagelschmitz and W. Jung, Chem. Mater. **10**, 3189 (1998).
[2] E. A. Nagelschmitz, W. Jung, R. Feiten, P. Müller, and H. Lueken, Z. Anorg. Allg. Chem. **627**, 523 (2001).
[3] U. Eibenstein and W. Jung, Z. Anorg. Allg. Chem. **624**, 802 (1998).
[4] R. Dronskowski and P. E. Blöchl, J. Phys. Chem. **97**, 8617 (1993).
[5] R. Dronskowski, K. Korczak, H. Lueken, and W. Jung, Angew. Chem., Int. Ed. **41**, 2528 (2002).
[6] R. Dronskowski, Adv. Solid State Phys. **42**, 433 (2002).
[7] O. N. Mryasov, U. Nowak, K. Y. Guslienko, and R. W. Chantrell, Europhys. Lett. **69**, 805 (2005).
[8] O. N. Mryasov, Phase Transitions **78**, 197 (2005).
[9] R. Y. Gu and V. P. Antropov, Phys. Rev. B **72**, 012403 (2005).
[10] S. Liu, Phys. Rev. B **15**, 4281 (1977).
[11] V. Korenman, J. L. Murray, and R. E. Prange, Phys. Rev. B **16**, 4032 (1977).
[12] A. Leichtenstein, M. Katsnelson, and V. Gubanov, J. Phys. F: Met. Phys. **14**, L125 (1984).
[13] A. Leichtenstein, M. Katsnelson, and V. Gubanov, Solid State Commun. **54**, 327 (1985).
[14] V. P. Antropov, J. Magn. Magn. Mater. **262**, L192 (2003).
[15] Y. Kurtulus, R. Dronskowski, G. D. Samolyuk, and V. P. Antropov, Phys. Rev. B **71**, 014425 (2005).
[16] R. Kikuchi, Phys. Rev. **81**, 988 (1951); V. G. Vaks and G. D. Samolyuk, J. Exp. Theor. Phys. **88**, 89 (1999).
[17] J. L. Xu, M. van Schilfgaarde, and G. D. Samolyuk, Phys. Rev. Lett. **94**, 097201 (2005).
[18] Y. Kurtulus, M. Gilleßen, and R. Dronskowski, J. Comput. Chem. **27**, 90 (2006).
[19] Y. B. Kuz'ma and O. I. Kripyakevich, Dopov. Akad. Nauk Ukr. RSR, Ser. A: Fiz.-Tekh. Mat. Nauki **31**, 939 (1969).
[20] O. Andersen, Phys. Rev. B **12**, 3060 (1975).
[21] O. K. Andersen and O. Jepsen, Phys. Rev. Lett. **53**, 2571 (1984).
[22] U. von Barth and L. Hedin, J. Phys. C **5**, 1629 (1972).
[23] J. P. Perdew, K. Burke, and M. Ernzerhof, Phys. Rev. Lett. **77**, 3865 (1996).
[24] M. van Schilfgaarde and V. Antropov, J. Appl. Phys. **85**, 4827 (1999).
[25] V. Antropov, B. Harmon, and A. Smirnov, J. Magn. Magn. Mater. **200**, 148 (1999).
[26] J. Callaway, A. K. Chatterjee, S. P. Singhal, and A. Ziegler, Phys. Rev. B **28**, 3818 (1983).
[27] J. F. Janak, Phys. Rev. B **16**, 255 (1977).
[28] J. van Vleck, Rev. Mod. Phys. **17**, 27 (1945).
[29] P. W. Anderson, in *Solid State Physics*, edited by F. Seitz and D. Turnball (Academic, New York, 1963), Vol. 17.
[30] F. Bloch, Z. Phys. **61**, 206 (1930).
[31] G. Landrum and R. Dronskowski, Angew. Chem., Int. Ed. **38**, 1389 (1999).
[32] L. E. Cox, J. W. Ward, and R. E. Haire, Phys. Rev. B **45**, 13239 (1992).
[33] B. P. T. Fokwa, H. Lueken, and R. Dronskowski, Chem.-Eur. J. **13**, 6040 (2007).
[34] D. C. Mattis, *The Theory of Magnetism* (Harpers & Row, New York, 1965).
[35] G. Cao, F. Freibert, and J. Crow, J. Appl. Phys. **81**, 3884 (1997).
[36] J. Villian, J. Phys. Chem. Solids **11**, 303 (1959); A. Yoshimori, J. Phys. Soc. Jpn. **14**, 807 (1959).
[37] O. K. Andersen, O. Jepsen, and D. Glotzel, in *Highlights of Condensed Matter Theory*, edited by F. Bassani, F. Fumi, and M. P. Tosi (North-Holland, Amsterdam, 1985), p. 59.
[38] V. P. Antropov, M. I. Katsnelson, B. N. Harmon, M. van Schilfgaarde, and D. Kusnezov, Phys. Rev. B **54**, 1019 (1996).
[39] A. Brooks Harris, Phys. Rev. **132**, 2398 (1963).